Author's Accepted Manuscript

www.elsevier.com/locate/talanta

A promising voltammetric biosensor based on glutamate dehydrogenase/Fe_3O_4/graphene/chitosan nanobiocomposite for sensitive ammonium determination in $PM_{2.5}$

Liangyun Yu, Qi Zhang, Dangqin Jin, Qin Xu, Xiaoya Hu

PII: S0039-9140(18)31366-3
DOI: https://doi.org/10.1016/j.talanta.2018.12.090
Reference: TAL19438

To appear in: *Talanta*

Received date: 17 July 2018
Revised date: 23 November 2018
Accepted date: 25 December 2018

Cite this article as: Liangyun Yu, Qi Zhang, Dangqin Jin, Qin Xu and Xiaoya Hu, A promising voltammetric biosensor based on glutamate dehydrogenase/Fe_3O_4/graphene/chitosan nanobiocomposite for sensitive ammonium determination in $PM_{2.5}$, *Talanta,* https://doi.org/10.1016/j.talanta.2018.12.090

A promising voltammetric biosensor based on glutamate dehydrogenase/Fe_3O_4/graphene/chitosan nanobiocomposite for sensitive ammonium determination in $PM_{2.5}$

Liangyun Yu[a,b,c], Qi Zhang[a,c], Dangqin Jin[d], Qin Xu[a,*], Xiaoya Hu[a,*]

[a]*College of Chemistry and Engineering, Yangzhou University, Yangzhou 225002, P. R. China*

[b]*College of Textiles and Clothing, Yancheng Institute of Technology, Yancheng 224051, P. R. China*

[c]*Jiangsu Collaborative Innovation Center for Ecological Building Materials and Environmental Protection Equipments, Yancheng Institute of Technology, Yancheng 224051, P. R. China*

[d]*Department of Chemical Engineering, Yangzhou Polytechnic Institute, Yangzhou 225127, P. R. China*

E-mail address: xuqin@yzu.edu.cn (Q. Xu),

xyhu@yzu.edu.cn (X. Hu).

**Corresponding author. Tel.: +86 514 87972034; Fax: +86 514 8975244.*

Abstract

A novel NH_4^+ voltammetric electrochemical biosensor was constructed by immobilizing glutamate dehydrogenase (GLDH)/Fe_3O_4/graphene (GR)/chitosan (CS) nanobiocomposite onto a glassy carbon electrode (GCE). On the GLDH/Fe_3O_4/GR/CS/GCE, GLDH catalyzed the reversible reaction, i.e., the reductive amination of α-ketoglutaric acid and the oxidative deamination of L-glutamate. The electrons produced in the enzymatic reactions were transferred to the surface of the electrode via the $[Fe(CN)_6]^{3-/4-}$ couple, which helped for the amplification of the electrochemical signal. The electrochemical detection of NH_4^+ was based on the fact that

the enhanced response current was proportional to the NH_4^+ concentration. Owing to the combination of the advantages of the synergistic effects of Fe_3O_4 nanospheres, GR and CS, a promising platform for NH_4^+ sensing was provided. Under optimum conditions, the introduced biosensor had a linear range of 0.4–2.0 μM for NH_4^+ with the detection and quantification limits of 0.08 and 0.27 μM, respectively. Moreover, the biosensor exhibited good sensitivity and excellent reproducibility. It could retain 91.8% of its original response after two weeks of storage at 4 °C, suggesting satisfactory stability. Additionally, the proposed biosensor was successfully applied to detect NH_4^+ levels in $PM_{2.5}$ samples, indicating its feasibility for application in NH_4^+monitoring in the environmental fields.

Graphical abstract

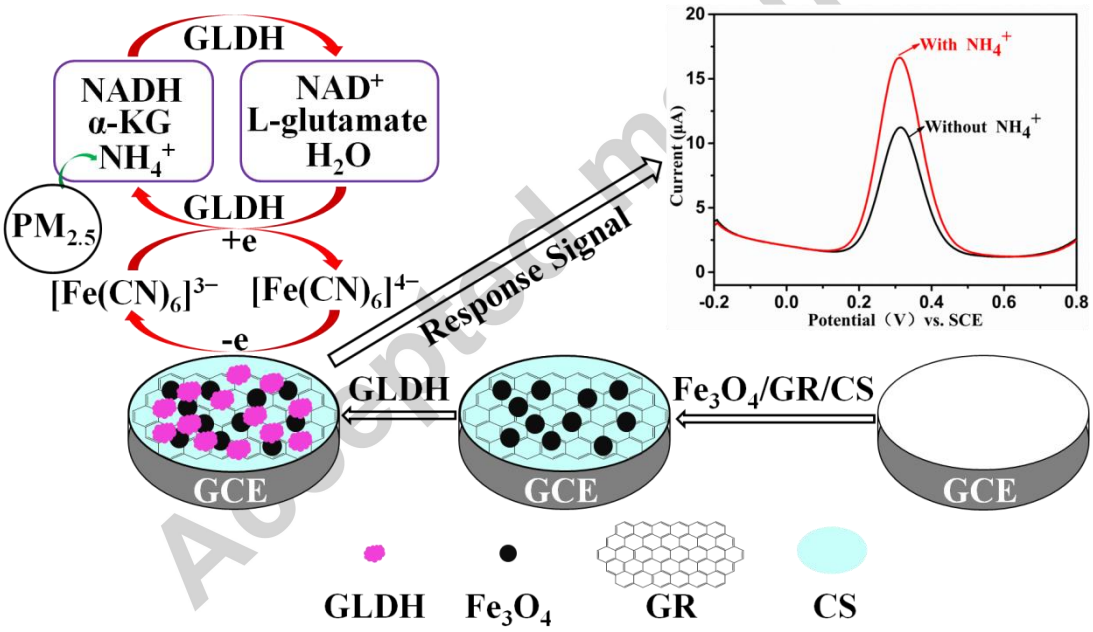

Keywords: Ammonium biosensor; Glutamate dehydrogenase; Fe_3O_4 nanospheres; Graphene; Chitosan; $PM_{2.5}$.

1. Introduction

Over the recent decades, air pollution has received extensive attention with the rapid development of industrialization and urbanization, as well as the continued growth of energy consumption and motor vehicles [1, 2]. Atmospheric aerosols, Atmospheric aerosols, especially fine aerosol particles $PM_{2.5}$ with the aerodynamic diameter no more than 2.5 μm have detrimental effects on air quality [3-5]. Ammonium (NH_4^+) is one of the main components of water-soluble inorganic ions, accounting for about one-third or more of the total $PM_{2.5}$ mass [6, 7]. Fine particle NH_4^+, such as $(NH_4)_2SO_4$, NH_4NO_3, and NH_4Cl are their common forms [8, 9], originates from local discharge, remote migration, and the chemical reaction between ammonia (NH_3) and nitric acid (HNO_3), sulfuric acid (H_2SO_4), or hydrochloric acid (HCl) [10]. Compared to NH_3, NH_4^+ has a longer lifetime of about 1−15 days and tends to deposit farther away from the emission source, leading to soil acidification, forest degradation and watercourse eutrophication [11]. It has great impacts on human health, environmental acidity, visibility, eutrophication and the biodiversity of ecosystems [12, 13]. Therefore, the quantitative assay of NH_4^+ in $PM_{2.5}$ is especially valuable for better understand its source, the formation mechanism of the secondary NH_4^+ aerosols, and the effective control of air pollution.

Accordingly, several techniques such as aerosol mass spectrometer (AMS), ion chromatography (IC), inductively coupled plasma mass spectrometry (ICPMS), particle into liquid sampler (PILS), and X-ray fluorescence (XRF) have been exploited [14, 15]. But they have some shortcomings such as complexity, high-cost, large size, time-consuming, poor portability and elaborate preparation procedures, which limit their widespread application. Thus,

it is highly necessary to develop a new simple, economical, reliable and efficient methodology for NH_4^+ assay in $PM_{2.5}$. Electrochemical strategies can meet this need owing to its simplicity, rapidness, sensitivity, reliability, low-cost and real-time analysis [16]. In this paper, we aimed to explore a novel voltammetric NH_4^+ biosensor based on the fact that the electrons produced in the reduction ammoniation of α-ketoglutaric acid (α-KG) and the oxidative deamination of L-glutamate under the catalysis of GLDH can transfer to the electrode surface by the $[Fe(CN)_6]^{3-/4-}$ couple resulting in enhanced current response.

Recently, nanomaterials have exerted a profound impact on the development of electrochemical biosensors and much effort has been invested in utilizing them to develop novel biosensors with rapid and sensitive response [17, 18]. In this context, exploiting nanomaterials to design an electrochemical biosensor for NH_4^+ assay in $PM_{2.5}$ with better performance seems to be very promising. Among the various nanomaterials, graphene is very popular because of its novel and unique properties (such as high electrical conductivity, excellent biocompatibility, special thermal and mechanical performance, etc.), and demonstrates tremendous application potentialities in fabricating various nanomaterial based electrochemical biosensors [19-21]. Graphene can promote the electron transfer of the proteins redox reaction and retain the enzymatic activity of the immobilized redox enzymes, so it has been utilized as a substrate for a variety of cells and biomolecules [22]. But graphene itself is a hydrophobic substance and without dispersants, it tends to form irreversible agglomerates or even graphite in aqueous solutions, hampering the exploration of its application [23]. As a consequence, the surface modification of graphene have gained a lot of intense research, and covalent or noncovalent functionalization of hydrophilic groups, polymer, aromatic molecule, or surfactant on the

graphene surface have so far been widely used, of which the noncovalent approaches are more advantageous than the covalent ones because the former won't destruct graphene's π-conjugated skeleton and loss of its electronic properties [24]. Polymers with hydrophobic tail and hydrophilic head have been employed for noncovalent functionalization of graphene via conjugation with its planar structure [25, 26]. Among a wide range of the polymer materials, chitosan (CS), the only basic polysaccharide in the natural polysaccharide produced by deacetylation of chitin, exhibits great potential for fabricating functional graphene nanocomposites in virtue of its remarkable properties such as good adhesion, good biocompatibility, nontoxicity, high water permeability and excellent membrane forming ability [27]. The CS and graphene nanocomposite materials can offer the high surface area for loading the enzymes and a compatible micro-environment for promoting the stability, but the use of CS poses a potential drawback that the formed non-conductive CS layer can hinder the diffusion of the analytes and may reduce the active area of biosensors, leading to lower sensitivity [22]. Fortunately, this shortcoming can be overcome by employing the biocompatible nanoparticles (NPs) such as Fe_3O_4 NPs, which have been exploited as a favorable immobilizing matrix for constructing biosensors owing to their high specific surface area, good biocompatibility, fast electron transfer capability, high adsorption performance, superparamagnetism and low toxicity [28]. Using magnetic nanoparticles to immobilize the bioactive molecules is very interesting because these magnetic bioconjugates may improve the transmissibility and reproducibility of biomolecules [29]. The aggregation of Fe_3O_4 NPs can also be improved by dispersing their NPs into the CS biopolymer matrix [30]. In addition, graphene nanocomposites show very favorable synergistic effects and have attracted extensive interest in many research fields, especially in the

construction of biosensors [31, 32]. Thus, the composites of Fe_3O_4 NPs, graphene and CS are a very good choice to build a good electrochemical biosensor platform.

Nonetheless, it is known that there have been no reports on the voltammetric detection of NH_4^+ based on the Fe_3O_4 nanospheres (NSs)/graphene/CS nanocomposite. In the present work, a new voltammetric biosensor of NH_4^+ was developed by immobilizing GLDH on this hybrid nanocomposite-modified glassy carbon electrode (GCE). Differential pulse voltammetry (DPV) was employed to study the performance of the biosensor. The synergistic effects of Fe_3O_4 NPs, graphene and CS are very helpful for the electrochemical sensing of NH_4^+. The newly fabricated biosensor exhibited high sensitivity, good reproducibility and stability, and satisfactory practical application.

2. Experiments section

2.1. Reagents and materials

Glutamate dehydrogenase from bovine liver (GLDH, type III, lyophilized powder, and ≥20 units/mg protein) and β-nicotinamide adenine dinucleotide (NADH) were procured from Sigma-Aldrich (USA). α-Ketoglutarate (α-KG) was bought from Tokyo Chemical Industry (Japan). Graphene (GR) was purchased from Nanjing Ji Cang Nano Technology Co., Ltd. (China). Methanesulfonic acid (MSA) was purchased from Energy Chemical (China). Polyvinylpyrrolidone (PVP), ferric chloride Iron (III) chloride hexahydrate, sodium acetate, sodium chloride, ethylene glycol, chitosan (CS) were bought from Sinopharm Chemical Reagent Co., Ltd (China). The 0.5 mg/mL CS solution was prepared by dissolving 50 mg CS in 100 mL acetic acid buffer solution (0.05 M, pH 4.2) and stored for several days to get a clear solution at ambient temperature. Phosphate buffers (PBS, 0.05 M) at different pH were achieved

by mixing different proportions of Na_2HPO_4 and NaH_2PO_4. Ammonium standard substance (1000 μg/mL) was purchased from China standard material procurement center. $PM_{2.5}$ samples collected on glass fabric filters by Met One instruments (BAM-1020, USA, 16.7 L/min) in the air pollution monitoring station of Yangzhou East Financial Institute were generously offered by Yangzhou Municipal Environmental Protection Bureau. Other chemicals not mentioned here were all of analytical grade and used directly. Aqueous solutions were prepared with ultrapure water (>18 MΩ·cm) throughout this work.

2.2 Apparatus

All electrochemical measurements were conducted at 25 °C on a CHI660D electrochemical analyzer (Shanghai CH Instruments, China) in PBS (0.05 M, pH 6.5, 0.9% NaCl) containing 0.02 mM $[Fe(CN)_6]^{3-/4-}$. A three-electrode system was employed, which consisted of a saturated calomel electrode (SCE) as the reference electrode, a platinum electrode as the auxiliary electrode, and a bare or modified glassy carbon electrode (GCE, Φ=3mm) as the working electrode. X-ray diffraction (XRD) characterization was performed on the D8 Advance diffractometer (Bruker-AXS, German) in the range of 2θ = 2−80° with Cu-Kα radiation (λ = 1.5418 Å or k = 0.154 06 nm). Vibrating sample magnetometer (EV7, ADE, USA) was employed to measure the superparamagnetism of Fe_3O_4 NSs. Fourier-transform infrared spectroscopy (FTIR, Nicolet iS10 instrument, USA), transmission electron microscopy (TEM, Philips Tecnai 12, Netherlands) and scanning electron microscopy (SEM, Hitachi S-4800, Japan) were adopted to investigate the changes in the structures and morphologies of the materials. High-resolution transmission electron microscopy (HRTEM) and energy dispersive X-ray (EDX) spectrum studies of Fe_3O_4/GR/CS were obtained using a Tecnai-G2 F30 S-TWIN microscope

(Philips, Netherlands) operated at 300 kV. Ion chromatography (IC, Dionex ICS-2000, USA) was adopted to assay NH_4^+ in $PM_{2.5}$ samples as a reference, which was equipped with an automatic eluent generator, a dual-piston pump, a column heater, an Ion Pac CS12A (4 mm × 250 mm) separation column, an Ion Pac CG12A (4 mm × 50 mm) guard column, a Dionex CSRS-300 (4 mm) suppressor, and a DS6 thermal conductivity detector. For the analysis of NH_4^+, 20 mM isocratic eluent of MSA and 1.0 mL min^{-1} eluent flow-rate were employed. The suppressor current was 70 mA. The injection volume was 20 μL. The column temperature was set at 30 °C. The total run time was about 10 min. The quantification was based on the chromatographic peak area.

2.3. Preparation of modified electrodes

Fe_3O_4 NSs were prepared by the solvothermal method as the previous literature [33]. The electrode modification began with polishing using 0.05 μm Al_2O_3 powder until the GCE surface was as smooth as a mirror. Then it was washed ultrasonically with ethanol and water for 3 min in turn and dried. The CS/GCE was obtained by casting 10 μL of 0.5 mg/mL CS solution on the surface of the pretreated GCE and then dried under the infrared light. The Fe_3O_4/CS/GCE was obtained by casting 10 μL of Fe_3O_4/CS suspension prepared by dispersing 1 mg Fe_3O_4 NSs in 1 mL of 0.5 mg/mL CS solution with the help of ultrasonication for about 4 h. The Fe_3O_4/GR/CS/GCE was prepared as the similar step by casting 10 μL of Fe_3O_4/GR/CS suspension which was obtained by dispersing 1 mg GR and 1 mg Fe_3O_4 NSs in 1 mL of 0.5 mg/mL CS solution with the help of ultrasonication for about 4 h.

For fabricating GLDH-based biosensors, 3 μL of 10 mg/mL GLDH in PBS (50 mM, pH 7.0) was coated on the CS/GCE, Fe_3O_4/CS/GCE, and Fe_3O_4/GR/CS/GCE respectively. The prepared

electrodes were rinsed with water, air-dried, and used as GLDH/CS/GCE, GLDH/Fe_3O_4/CS/GCE, and GLDH/Fe_3O_4/GR/CS/GCE. After the modification, the modified electrodes were kept at 4 °C in the refrigerator when not in use.

2.4 Electrochemical measurement

The fabricated biosensor was immersed in 10 mL of PBS (0.05 M, pH 6.5, 0.9% NaCl) containing 0.02 mM $[Fe(CN)_6]^{3-/4-}$ in the presence of NADH (0.034 mM) and α-KG (1.5 mM). The redox couple of $[Fe(CN)_6]^{3-/4-}$ was recorded using DPV at the potential range from –0.2 to 0.8 V (vs. SCE) with pulse amplitude 50 mV, pulse width 50 ms, potential increment 4 mV, and quiet time 3 s. For the electrochemical experiments, the DPV of the blank solution was monitored firstly. Then the DPV was run again after aliquots of NH_4^+ were injected to the above solution with gently agitation. On the GLDH/Fe_3O_4/GR/CS/GCE, GLDH catalyzed the reversible reaction, i.e., the reductive amination of α-KG and the oxidative deamination of L-glutamate. The electrons produced by these enzymatic reactions were transferred to the surface of the electrode via the $[Fe(CN)_6]^{3-/4-}$ couple resulting in increased electrochemical signal. The electrochemical measurement of NH_4^+ was achieved based on its concentration vs. the enhanced current.

2.5 Treatment of real samples

According to the literature [34], the treatment process of the real samples included several steps. Firstly, 10mL ultrapure water was added to 24-h $PM_{2.5}$ filter samples. Secondly, the mixture was extracted ultrasonically for half an hour with the temperature no more than 30 °C. Thirdly, the extract was collected and the previous process was repeated. Fourthly, the two extracts were combined and filtered through a 0.22 μm membrane filer. Finally, the filtrate was

preserved in the refrigerator for further analysis.

3. Results and discussion

3.1 Characterization of the materials and the proposed biosensor

Fig. 1A displays the XRD patterns of GR (curve a), CS (curve b), Fe_3O_4 NSs (curve c) and Fe_3O_4/GR/CS nanocomposite (curve d). The diffraction pattern of GR comprised diffraction peaks from the (002), (100), (101) and (004) crystallographic planes at the corresponding 2θ values of 26.38°, 42.22°, 44.39° and 54.54° [JCPDS card no. 41-1487]. The XRD spectrum of CS showed a strong diffraction peak at 2θ value of 20.18° due to (110) crystallographic plane [35]. As for the XRD spectrum of the pure Fe_3O_4 NSs, a series of diffraction peaks located at 2θ values of 30.0° (220), 35.4° (311), 43.2° (400), 53.3° (422), 57.1° (511), 62.7° (440) and 74.1° (553) were observed, which was in good agreement with the cubic spinel crystal structure of Fe_3O_4 (JCPDS card no. 19-629) [33, 36, 37]. The average size of the crystal was calculated to be 16.7 nm using Debye-Scherrer equation. As described in literature [33], it indicated that the synthesized Fe_3O_4 NSs were mainly composed of the particles of around 17 nm in diameter, which would be further confirmed by the following characterization. The diffraction pattern of Fe_3O_4/GR/CS hybrid nanocomposite comprised diffraction peaks from the (110) crystallographic plane of CS, the (002) and (004) crystallographic planes of GR, and the (220), (311), (400), (422), (511), (440) and (533) crystallographic planes of Fe_3O_4 NSs. Although the peaks for GR at 2θ values of 42.22° and 44.39° were shielded and the peak for CS at 2θ values of 20.18° was weakened after being combined, it was enough to prove that they have been compounded together with Fe_3O_4 NSs successfully.

Fig. 1B shows the magnetization hysteresis loops of Fe_3O_4 NSs investigated at room

temperature. Obviously, one S-like curve was presented and the saturation magnetization (Ms) of Fe_3O_4 NSs was 85.5 emu/g, which was closer to 92.0 emu/g of the bulk Fe_3O_4 [38], and the coercivity value (Hc) was 23.98 Oe, indicating the weak ferromagnetism of Fe_3O_4 NSs. It could be explained that larger Fe_3O_4 NSs were formed through the accumulation of many primary Fe_3O_4 NPs which would be confirmed by the following TEM characterization. These accumulations made them similar to block magnets and showed higher Ms than those individual primary particles [33].

{Insert Fig. 1 here}

Fig. 2A-C shows the TEM images of Fe_3O_4 NSs (A), GR (B) and Fe_3O_4/GR/CS (C). As can be seen, the prepared Fe_3O_4 NSs were formed by the aggregation of a lot of small Fe_3O_4 NPs which exhibited well-defined spheroidal structures and crude surfaces with average diameter of around 400 nm. The large size of Fe_3O_4 NSs has been owing to the aggregation of a lot of small Fe_3O_4 NPs. Fig. 2D and E illustrate the HRTEM images of Fe_3O_4/GR/CS nanocomposite, which further proved the aggregation of small Fe_3O_4 NPs and their aggregates were distributed on the GR sheets. The d-spacing of about 0.297 and 0.253 nm corresponded well to the (220) and (311) lattice planes of Fe_3O_4 NSs respectively, and that of 0.216 nm belonged to the (100) face of GR, which indicated the crystalline structure of Fe_3O_4 NSs and GR. The inset in Fig. 2E exhibits the selected area electron diffraction (SEAD) pattern of Fe_3O_4/GR/CS nanocomposite. The Miller indices matched well agreed with the XRD pattern. Fig. 2F demonstrates the EDX spectrum of Fe_3O_4/GR/CS and the Fe, O and C atoms were clearly observed. Therefore, it was reasonable to conclude that the Fe_3O_4/GR/CS nanocomposite had been synthesized successfully.

{Insert Fig. 2 here}

Fig. 3A-E exhibits the SEM images of CS/GCE (A), Fe_3O_4/CS/GCE (B), GR/CS/GCE (C), Fe_3O_4/GR/CS/GCE (D), and GLDH/Fe_3O_4/GR/CS/GCE (E). Obviously, Fe_3O_4/GR/CS could be tightly adhered to the GCE surface to form a net-like film, indicating the incorporation of Fe_3O_4 NSs, GR in CS. The formation of Fe_3O_4/GR/CS hybrid nanocomposite might be ascribed to the electrostatic interactions between the negatively charged GR, Fe_3O_4 NSs and the cationic CS [39]. Also, the uniform distribution of Fe_3O_4 NSs on the related electrodes could be attributed to the synergic effect between the three materials employed. The Fe_3O_4/GR/CS hybrid provided a favorable circumstance for high-load immobilization of enzyme, and the smooth morphology of GLDH/Fe_3O_4/GR/CS/GCE indicated that GLDH had been immobilized on the Fe_3O_4/GR/CS hybrid. These results were further supported by the FTIR and electrochemical studies.

Fig. 3F displays the FTIR spectra of CS (curve a), Fe_3O_4 (curve b), Fe_3O_4/CS (curve c), Fe_3O_4/GR/CS (curve d), and GLDH/Fe_3O_4/GR/CS (curve e). The FTIR spectrum of CS (curve a) demonstrated the stretching vibrations of –OH and $–NH_2$ at 3447 cm^{-1}, the stretching vibrations of $–CH_3$ and $–CH_2–$ at 2920 and 2876 cm^{-1} respectively, the amide I group at 1657 and 1599 cm^{-1}, the C–N axial deformation at 1425 cm^{-1}, the stretching vibration of COO^- at 1383 cm^{-1}, the peak of β (1–4) glycoside in polysaccharide unit at 1157 cm^{-1}, the stretching vibration of C–OH at 1082 cm^{-1} and the stretching vibration of C–O–C on glucose ring at 1024 cm^{-1} [29]. The FTIR spectrum of Fe_3O_4 (curve b) exhibited the peak at 3422 cm^{-1} belonged to –OH stretching vibration and the peak at 588 cm^{-1} due to the Fe–O vibration, which confirmed the presence of Fe_3O_4 [40]. The FTIR spectra of Fe_3O_4/CS (curve c), Fe_3O_4/GR/CS (curve d), and GLDH/Fe_3O_4/GR/CS (curve e) showed peaks corresponding to the pure CS and bare Fe_3O_4. The

stretching vibration absorption peaks of –OH and $–NH_2$ appeared at lower wave number, and the peak intensity of Fe–O stretching changed, indicating the combination of the amine group of CS with Fe_3O_4 NSs via electrostatic interactions. Moreover, the characteristic infrared peaks assigned to GR can also be found in curve d and e, such as the enhanced peak of C=C skeletal vibrations at 1574 cm^{-1}, the peaks of epoxy and alkoxy C–O vibration at 1262 cm^{-1} and 924 cm^{-1} respectively [41], indicating the formation of Fe_3O_4/GR/CS hybrid nanocomposite. Meanwhile, the shape of GLDH/Fe_3O_4/GR/CS absorption peak became broader due to the overlap of the characteristic peaks of GLDH and Fe_3O_4/GR/CS nanocomposite film, demonstrating GLDH being successfully immobilized in the nanocomposite matrix [39].

3.2 Electrochemical response studies of the biosensor

Fig. 4A demonstrates the DPVs recorded respectively on the bare GCE (curve a), CS/GCE (curve b), Fe_3O_4/CS/GCE (curve c), GR/CS/GCE (curve d), Fe_3O_4/GR/GCE (curve e), Fe_3O_4/GR/CS/GCE (curve f) and GLDH/Fe_3O_4/GR/CS/GCE (curve g) in 10 mL of PBS (0.05 M, pH 6.5, 0.9% NaCl) containing 0.02 mM $[Fe(CN)_6]^{3-/4-}$. As shown, the response current of the CS/GCE was 8.67 times that of the bare GCE, which could be owing to the cationic CS accepting electrons from $[Fe(CN)_6]^{3-/4-}$. When Fe_3O_4 NSs were incorporated into CS (curve c), the peak currents were continued to increase by 72.06%. This was because the magnetic Fe_3O_4 NSs could induce magnetization in the electrical field, leading to uniform dispersion of Fe_3O_4 NSs throughout CS network on the surface of the electrode and facilitating the flow of electrons [39, 42]. On the other hand, the current response of the GR/CS/GCE (curve d) was increased by 102.14% compared with the CS/GCE, which could be owing to the large specific surface area

and high electrical conductivity of GR. When the electrode was modified with Fe_3O_4/GR (curve e), the current response of the modified electrode was increased by 46.82% compared with the GR/CS/GCE, indicating the excellent properties of Fe_3O_4 NSs. Moreover, the significant enhancement in the response currents was observed on the Fe_3O_4/GR/CS/GCE (curve f). The current increased by 40.46% over the Fe_3O_4/GR/GCE, which might be attributed to the synergistic effects between each constituent. However, after the immobilization of GLDH (curve g), the response signal was reduced by 39.27%, suggesting that the enzyme was firmly immobilized onto the surface of Fe_3O_4/GR/CS/GCE. It might be due to the insulativity of GLDH blocking the transfer of electrons between the medium and the electrode. The above results suggested that the prepared Fe_3O_4/GR/CS nanocomposite had excellent performance and could provide a biocompatible environment for GLDH.

Meanwhile, electrochemical impedance spectroscopy (EIS) was employed to further characterize the behavior of the preparation and assembly process of the biosensor. And the charge transfer resistances (Rct) of each modified step were monitored in 5.0 mM $[Fe(CN)_6]^{3-/4-}$ as the redox probe with 0.1 M KCl as the supporting electrolyte. Fig. 4B shows the Nyquist plots of the bare GCE (curve a), CS/GCE (curve b), Fe_3O_4/CS/GCE (curve c), GR/CS/GCE (curve d), Fe_3O_4/GR/GCE (curve e), Fe_3O_4/GR/CS/GCE (curve f) and GLDH/Fe_3O_4/GR/CS/GCE (curve g). According to the semicircle diameters of Nyquist plots, the Rct values for various electrodes were estimated. As is shown, comparing with a relatively large Rct of 296 Ω on the bare GCE, smaller semicircles of 209 Ω on the CS/GCE, 158 Ω on the Fe_3O_4/CS/GCE, 121 Ω on the GR/CS/GCE, 74 Ω on the Fe_3O_4/GR/GCE, 34 Ω on the Fe_3O_4/GR/CS/GCE and 100 Ω on GLDH/Fe_3O_4/GR/CS/GCE were obtained respectively. The

significantly reduced Rct could be mainly attributed to the enlarged specific surface area and the high electrical conductivity, which promoted the electron transfer and mass exchange of the electroactive indicators on the electrode surface. It indicated that the enhancement effect of CS, Fe_3O_4 NSs and GR on the response current of GCE increased successively, and the combination of these three materials played a synergistic effect, which greatly increased the electron transfer rate on the electrode surface. So it could be drawn from the results that Fe_3O_4/GR/CS nanocomposite effectively integrated the excellent properties of Fe_3O_4 NSs, GR and CS, and was a promising candidate for the construction of the high-performance electrochemical sensors.

The inset of Fig. 4A shows the DPVs of GLDH/Fe_3O_4/GR/CS/GCE in the absence (curve a) or presence (curve b and c) of NH_4^+ in the same blank solution as above with 0.034 mM NADH and 1.5 mM α-KG. It could be noted that the response signals at about 0.3 V increased with the increases of NH_4^+ concentrations. Fig. 5 illustrates the mechanism of the increase of the electrochemical current. GLDH can catalyze the transformation of NADH, NH_4^+ and α-KG into NAD^+, L-glutamate and H_2O by the reductive amination of α-KG. Meanwhile, the oxidative deamination of L-glutamate can also occur by the catalysis of GLDH. The electrons generated during the enzymatic reactions were transferred to the surface of GLDH/Fe_3O_4/GR/CS/GCE through the $[Fe(CN)_6]^{3-/4-}$ couple, which helped for the amplification of the current signal, resulting in improved sensitivity of the biosensor. The quantification of NH_4^+ in the present work was based on the fact that the electrochemical current was linearly related to the concentration of NH_4^+.

3.3 Parameter optimization

The effect of pH on the performance of the biosensor in the range of 5.0–9.0 was studied. Results shown in Fig. 6A indicated that the biosensor response was pH dependent, and the maximum current response was obtained at pH 6.5. The increase of pH could improve the biosensor's stability. But at the same time it would reduce the electron transfer, which would eventually lead to decrease in the response current of the biosensor [43]. Although the optimum activity of GLDH was found at pH 8.5, it still had relatively high activity and stability at pH 6.5 [44]. It was worth mentioning that the use of ferricyanide in the electrochemical process and the polymer matrix used for immobilization might also affect the optimal pH [45]. Additionally, the response current at pH 8.5 was much smaller than at pH 6.5. So we chose the optimal pH of 6.5.

The amount of enzyme can affect the performance of the constructed biosensor. Fig. 6B depicted the variation of the current response with the load of GLDH. With the increase of GLDH loading, the response current increased rapidly to reach a peak value at 0.03 mg. However, continuing to increase the amount of GLDH would increase the steric resistance and the non-specific adsorption of GLDH on Fe_3O_4/GR/CS nanocomposites. Therefore, 0.03 mg GLDH was employed for the fabrication of the biosensor.

The effect of the concentration of NADH on the performance of the biosensor was next evaluated, as shown in Fig. 6C. The response signal increased with increasing concentration of NADH and reached the maximum value at the concentration of 0.34 mM. When it was above 0.34 mM, a decrease in the response current was observed. It could be explained that an overdose of NADH might inhibit the enzyme activity competitively. Accordingly, the optimum concentration of NADH was 0.34 mM.

The effect of the concentration of α-KG on the biosensor performance was also examined in the concentration range of 0.05–3.0 mM. As seen in Fig. 6D, the response current increased with increasing concentration of α-KG and the optimum value was obtained at 1.5 mM. And further increase of the α-KG concentration resulted in small change in the response current. Thus, 1.5 mM of α-KG was used for all further studies.

3.4. Calibration of the biosensor

GLDH/Fe_3O_4/GR/CS/GCE was employed for NH_4^+ detection by DPV under the above optimal conditions. The DPV responses and the calibration curve were achieved in Fig. 7. It displayed that the response signal had a linear relationship with the concentration of NH_4^+ from 0.4–2.0 μM. The linearization equation was I (μA) = 12.9992 + 1.8746 C (μM) with the correlation coefficient of 0.9988. The limit of detection (LOD) and the limit of quantification (LOQ) calculated from the calibration curves as kSD/b (k=3 for LOD, k=10 for LOQ, SD is the standard deviation of the intercept, b is the slope of the calibration curve) [46] were 0.08 μM and 0.27 μM, respectively. Table 1 summarized the comparison of the performance of GLDH/Fe_3O_4/GR/CS/GCE with other GLDH-based NH_4^+ biosensors which have been reported in the literatures. As is shown, the analytical performance of the proposed sensor was competitive because it presented the lower detection limit than that of all other sensing strategies listed in the table. It should be owing to the enlarged effective surface area and the promoted electron transfer rate provided by the Fe_3O_4/GR/CS film. Although the new biosensor had relatively narrow linear response range as some biosensors based on GLDH [50-52], it could be applied to the detection of NH_4^+.

3.5 Specificity, reproducibility and stability

To examine the selectivity of the proposed biosensor, the interference measurements were carried out by DPV in the selected experiment conditions in the presence of 1.0 μM NH_4^+. The results revealed that the addition of other water-soluble ions usually coexistent in $PM_{2.5}$ samples including water-soluble inorganic ions of K^+, Na^+, Ca^{2+}, Mg^{2+}, SO_4^{2-}, NO_3^-, PO_4^{3-}, F^-, and Cl^- (each 50 μM) and water-soluble organic ions of formate, acetate, MSA, oxalate, malonate, succinate, suberate, sebacate and p-phthalate (each 10 μM) exhibited a deviation on the response currents less than ±5%, indicating the specificity of the constructed biosensor. In other words, this biosensor was highly selective in determining NH_4^+ under the optimum experiment conditions and could be applied to NH_4^+ detection in $PM_{2.5}$ samples.

Next, the reproducibility and stability of the prepared biosensor was examined. The relative standard deviation (RSD) of eight successive DPV measurements of the same electrode was less than 3.3% at the optimal conditions in the presence of 1.0 μM NH_4^+. Six parallel prepared electrodes were also performed the DPV measurements under the same conditions, and the RSD was estimated to be 2.6%. The above results showed that the biosensor had good reproducibility. When not in use, the modified electrode was stored at 4 °C. After two weeks deposit, it could retain 91.8% of its original current, indicating good storage stability.

3.6. Application in real sample

To investigate the feasibility of the new biosensor in practical application, the DPV experiments were carried out under the optimal experimental conditions to detect NH_4^+ content in $PM_{2.5}$ samples by the standard addition method. The NH_4^+ sample solution was extracted

from $PM_{2.5}$ samples as described in Section 2.5. The results of the quantification by the proposed electrochemical method and the standard method of IC, together with the recovery study, were summarized in Table 2. As shown, good percent recovery (between 100.8% and 102.0%) was provided, indicating the sufficient effectiveness of the biosensor in determining NH_4^+ content in $PM_{2.5}$ samples. Moreover, the NH_4^+ contents obtained by the proposed biosensor were well consistent with those data determined by IC, which further revealed the accuracy and reliability of the present method for NH_4^+ monitoring campaigns.

4. Conclusion

Fe_3O_4 NSs and GR have been combined in CS matrix to prepare nanocomposite for the immobilization of GLDH. Based on the GLDH/Fe_3O_4/GR/CS/GCE, the mediated voltammetric biosensor for NH_4^+ determination was successfully developed. It exhibited that the presence of Fe_3O_4/GR/CS nanocomposite resulted in enhanced performance to the constructed biosensor. In the analysis system, GLDH catalyzed the reversible reaction, i.e., the reductive amination of α-KG and the oxidative deamination of L-glutamate. Compared with the existing methods, the introduced biosensor displayed low detection limits (LOD and LOQ of 0.08 and 0.27 μM, respectively), a simple detection procedure, good selectivity and reproducibility. Moreover, the as-made biosensor was successfully applied to determine NH_4^+ in $PM_{2.5}$ by verification of IC, indicating its suitability for application in NH_4^+ monitoring in the environmental fields.

Acknowledgments

The authors gratefully acknowledge NSFC (No. 21575124, 21675140, 21275124 and 21275125), the PAPD of Jiangsu Higher Education Institutions, the Fund of Yangzhou City of

Environmental Protection Bureau (YHK1409 and YHK1410), the high-end talent project of Yangzhou University, the 14th Six talent peaks project in Jiangsu Province (SWYY-085), the Natural Science Research Project of Jiangsu Higher Education (17KJD150007 and 16KJB150044), Colleges and Universities in Jiangsu Province College Students' Innovative Entrepreneurial Training Program (2018), the Higher Education Outstanding Scientific and Technological Innovation Team of Jiangsu Province (2017-6), the Young academic leaders of Jiangsu Province (2018), the 333 high-level talent training project (2016-7, BRA2017479). We also thank the Test Center of Yangzhou University for SEM, TEM and other characterizations.

References

[1] G. Li, C. Fang, S. Wang, S. Sun, Environ. Sci. Technol., 50 (2016) 11452-11459.

[2] T. Huang, J. Chen, W. Zhao, J. Cheng, S. Cheng, Atmosphere, 7 (2016).

[3] Y. Xia, J. Tao, L. Zhang, R. Zhang, S. Li, Y. Wu, J. Cao, X. Wang, Q. Ma, Z. Xiong, Sci. Total Environ., 587 (2017) 240-247.

[4] G. Duporté, J. Parshintsev, L.M.F. Barreira, K. Hartonen, M. Kulmala, M.-L. Riekkola, Environ. Sci. Technol., 50 (2016) 4693-4700.

[5] Y. Zou, C. Jin, Y. Su, J. Li, B. Zhu, Environ. Pollut., 212 (2016) 627-635.

[6] B. Han, R. Zhang, W. Yang, Z. Bai, Z. Ma, W. Zhang, Sci. Total Environ., 544 (2016) 319-329.

[7] L. Wang, D. Ji, Y. Li, M. Gao, S. Tian, T. Wen, Z. Liu, L. Wang, P. Xu, C. Jiang, Y. Wang, Atmos. Res., 192 (2017) 19-29.

[8] M. Zhao, S. Wang, J. Tan, Y. Hua, D. Wu, J. Hao, Aerosol. Air Qual. Res., 16 (2016) 1378-1389.

[9] S. Wang, J. Nan, C. Shi, Q. Fu, S. Gao, D. Wang, H. Cui, A. Saiz-Lopez, B. Zhou, Sci. Rep., 5 (2015) 1-13.

[10] W. Wang, S. Wang, J. Xu, R. Zhou, C. Shi, B. Zhou, Environ. Sci. Pollut. Res., 23 (2016) 1691-1702.

[11] A. Ianniello, F. Spataro, G. Esposito, I. Allegrini, M. Hu, T. Zhu, Atmos. Chem. Phys., 11 (2011) 10803-10822.

[12] O. Hertel, C.A. Skjoth, S. Reis, A. Bleeker, R.M. Harrison, J.N. Cape, D. Fowler, U. Skiba, D. Simpson, T. Jickells, M. Kulmala, S. Gyldenkaerne, L.L. Sorensen, J.W. Erisman, M.A. Sutton, Biogeosciences, 9 (2012) 4921-4954.

[13] Q.-F. Li, L. Wang-Li, S.B. Shah, R.K.M. Jayanty, P. Bloomfield, Environ. Sci. Pollut. Res., 21 (2014) 4675-4685.

[14] J.-S. Kim, A.L. Bais, S.-h. Kang, J. Lee, K. Park, J. Atmos. Chem., 68 (2011) 251-263.

[15] S. Long, J. Zeng, Y. Li, L. Bao, L. Cao, K. Liu, L. Xu, J. Lin, W. Liu, G. Wang, J. Yao, C. Ma, Y. Zhao, J. Environ. Sci., 26 (2014) 1040-1051.

[16] S. Radhakrishnan, K. Krishnamoorthy, C. Sekar, J. Wilson, S.J. Kim, Chem. Eng. J., 259 (2015) 594-602.

[17] Z. Zhu, Nano-Micro Letters, 9 (2017).

[18] Q. Sheng, X. Qiao, M. Zhou, J. Zheng, Microchim. Acta, 184 (2017) 1573-1585.

[19] T. Kuila, S. Bose, P. Khanra, A.K. Mishra, N.H. Kim, J.H. Lee, Biosens. Bioelectron., 26 (2011) 4637-4648.

[20] C. Shan, H. Yang, D. Han, Q. Zhang, A. Ivaska, L. Niu, Biosens. Bioelectron., 25 (2010) 1070-1074.

[21] Y. Wang, H. Sauriat-Dorizon, H. Korri-Youssoufi, Sens. Actuators, B, 251 (2017) 40-48.

[22] J. Singh, P. Khanra, T. Kuila, M. Srivastava, A.K. Das, N.H. Kim, B.J. Jung, D.Y. Kim, S.H. Lee, D.W. Lee, D.-G. Kim, J.H. Lee, Process Biochem., 48 (2013) 1724-1735.

[23] X. Fang, J. Liu, J. Wang, H. Zhao, H. Ren, Z. Li, Biosens. Bioelectron., 97 (2017) 218-225.

[24] H. Liu, J. Gao, M. Xue, N. Zhu, M. Zhang, T. Cao, Langmuir, 25 (2009) 12006-12010.

[25] K.K. Reza, M.A. Ali, M.K. Singh, V.V. Agrawal, A.M. Biradar, Microchim. Acta, 184 (2017) 1809-1816.

[26] J. Zhang, J. Lei, R. Pan, Y. Xue, H. Ju, Biosens. Bioelectron., 26 (2010) 371-376.

[27] J. Liu, X. Wang, T. Wang, D. Li, F. Xi, J. Wang, E. Wang, ACS Appl. Mater. Interfaces, 6 (2014) 19997-20002.

[28] T. Madrakian, S. Maleki, M. Heidari, A. Afkhami, Mater. Sci. Eng. C Mater. Biol. Appl., 63 (2016) 637-643.

[29] A. Kaushik, R. Khan, P.R. Solanki, P. Pandey, J. Alam, S. Ahmad, B.D. Malhotra, Biosens. Bioelectron., 24 (2008) 676-683.

[30] A. Kaushik, P.R. Solanki, A.A. Ansari, B.D. Malhotra, S. Ahmad, Biochem. Eng. J., 46 (2009) 132-140.

[31] A. Noorbakhsh, M. Khakpoor, M. Rafieniya, E. Sharifi, M. Mehrasa, Electroanalysis, 29 (2017) 1113-1123.

[32] F. Fartas, J. Abdullah, N. Yusof, Y. Sulaiman, M. Saiman, Sensors, 17 (2017).

[33] M. Zhu, G. Diao, J. Phys. Chem. C, 115 (2011) 18923-18934.

[34] X.C. Yu, K.B. He, Y.L. Ma, F.M. Yang, F.K. Duan, A.H. Zheng, C.Y. Zhao, J. Environ. Sci., 16 (2004) 813-815.

[35] A. Jbeli, Z. Hamden, S. Bouattour, A.M. Ferraria, D.S. Conceicao, L.F.V. Ferreira, M.M. Chehimi, A.M.B. do Rego, M. Rei Vilar, S. Boufi, Carbohydr. Polym., 199 (2018) 31-40.

[36] J. Qian, X. Yang, L. Jiang, C. Zhu, H. Mao, K. Wang, Sens. Actuators, B, 201 (2014) 160-166.

[37] Y. Li, X. Zhao, P. Li, Y. Huang, J. Wang, J. Zhang, Anal. Chim. Acta, 884 (2015) 106-113.

[38] J. Liu, J. Wei, S. Li, Mater. Lett., 61 (2007) 1529-1532.

[39] A. Kaushik, P.R. Solanki, A.A. Ansari, G. Sumana, S. Ahmad, B.D. Malhotra, Sens. Actuators, B, 138 (2009) 572-580.

[40] M.A. Habila, Z.A. Alothman, A.M. El-Toni, J.P. Labis, M. Soylak, Talanta, 154 (2016) 539-547.

[41] L. Yu, Q. Xu, D. Jin, Q. Zhang, A. Mao, Y. Shu, B. Yan, X. Hu, Chem. Eng. J., 294 (2016) 122-131.

[42] R. Singh, R. Verma, A. Kaushik, G. Sumana, S. Sood, R.K. Gupta, B.D. Malhotra, Biosens. Bioelectron., 26 (2011) 2967-2974.

[43] P. Bertocchi, D. Compagnone, G. Palleschi, Biosens. Bioelectron., 11 (1996) 1-10.

[44] F. Ren, L. Chen, Q. Tong, Trop. J. Pharm. Res., 13(12) (2014) 2075-2082.

[45] R. Monošík, M. Streďanský, E. Šturdík, Food Anal. Methods, 6 (2013) 521-527.

[46] S. Smarzewska, W. Ciesielski, Food Analytical Methods, 8 (2014) 635-642.

[47] J.P. Hart, S. Serban, L.J. Jones, N. Biddle, R. Pittson, G.A. Drago, Anal. Lett., 39 (2006) 1657-1667.

[48] K.S.H. J.K. Yang, H.S. Baek, S.S. Lee, M.L. Seo, Bull. Korean Chem. Soc., 25(10) (2004) 1499-1502.

[49] S. Poorahong, P. Santhosh, G.V. Ramirez, T.F. Tseng, J.I. Wong, P. Kanatharana, P. Thavarungkul, J. Wang, Biosens. Bioelectron., 26 (2011) 3670-3673.

[50] S.A. Rahman, J. Abdullah, N.E.A. H. Sidek, Anal. Bioanal. Electrochem., 4(3) (2012) 262-276.

[51] A.K. Abassa, J.P. Harta, D.C. Cowell, A. Chappell, Anal. Chim. Acta., 373 (1998) 1-8.

[52] R.C.H. Kwan, P.Y.T. Hon, R. Renneberg, Sens. Actuators, B, 107 (2005) 616-622.

Legends of Figures

Fig. 1(A) XRD patterns of (a) GR, (b) CS, (c) Fe_3O_4 NSs and (d) Fe_3O_4/GR/CS nanocomposite. (B) Magnetic hysteresis curve and enlarged partial curve (insert in B) of Fe_3O_4 NSs.

Fig. 2 TEM images of (A) Fe_3O_4 NSs, (B) GR and (C) Fe_3O_4/GR/CS nanocomposite. HRTEM images (D and E), SEAD pattern (insert in E) and EDX spectrum (F) of Fe_3O_4/GR/CS nanocomposite.

Fig. 3 SEM images of (A) CS/GCE, (B) Fe_3O_4/CS/GCE, (C) GR/CS/GCE, (D) Fe_3O_4/GR/CS/GCE and (E) GLDH/Fe_3O_4/GR/CS/GCE. (F) FTIR spectra of (a) CS, (b) Fe_3O_4, (c) Fe_3O_4/CS, (d) Fe_3O_4/GR/CS and (e) GLDH/Fe_3O_4/GR/CS.

Fig. 4(A) DPVs of (a) the bare GCE, (b) CS/GCE, (c) Fe_3O_4/CS/GCE, (d) Fe_3O_4/GR/CS/GCE and (e) GLDH/Fe_3O_4/GR/CS/GCE in 0.05 M PBS (pH 6.5) containing 0.9% NaCl and 0.02 mM $[Fe(CN)_6]^{3-/4-}$. Inset: DPVs of GLDH/Fe_3O_4/GR/CS/GCE in the presence of 0.034 mM NADH and 1.5 mM α-KG with (a) 0, (b) 1 and (c) 2 μM NH_4^+ buffered with the same solution as above. (B) Nyquist plots recorded for (a) the bare GCE, (b) CS/GCE, (c) Fe_3O_4/CS/GCE, (d) GR/CS/GCE, (e) Fe_3O_4/GR/GCE, (f) Fe_3O_4/GR/CS/GCE and (g) GLDH/Fe_3O_4/GR/CS/GCE in

5.0 mM $[Fe(CN)_6]^{3-/4-}$ with 0.1 M KCl as a supporting electrolyte.

Fig. 5 Schematic diagram of the electrochemical detection of NH_4^+ by the biosensor.

Fig. 6 The effect of pH, the amount of GLDH, the NADH and α-KG concentrations on the performance of the biosensor.

Fig. 7 DPVs of GLDH/Fe_3O_4/GR/CS/GCE as a function of NH_4^+concentration (0.4–2.0 μM) in 0.05 M PBS (pH 6.5) containing 0.9% NaCl and 0.02 mM $[Fe(CN)_6]^{3-/4-}$ in the presence of 0.034 mM NADH and 1.5 mM α-KG. Inset: the calibration curve.

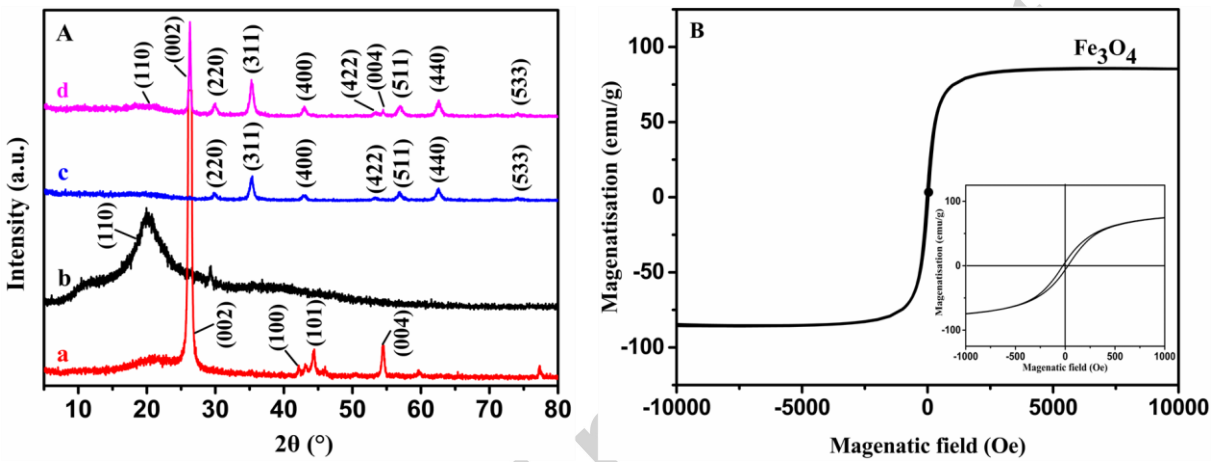

Fig. 1

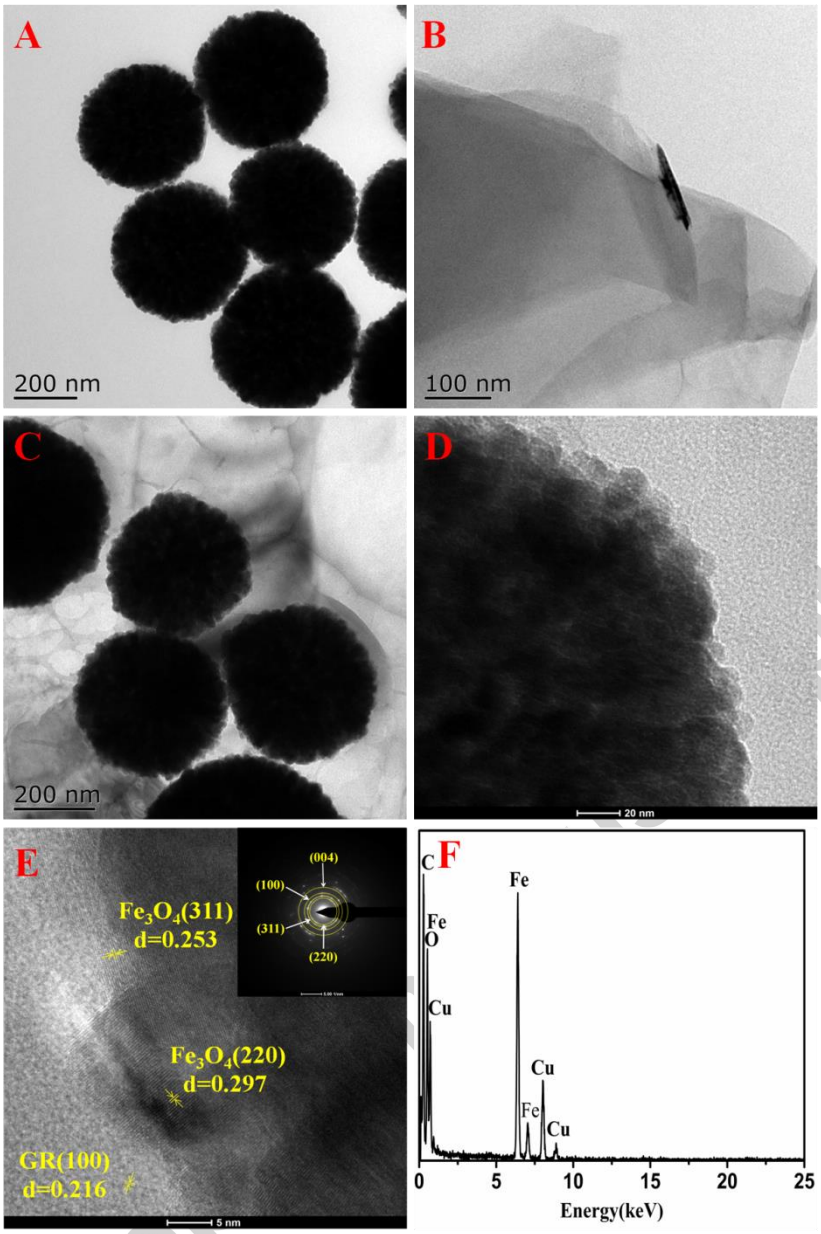
A
200 nm
B
100 nm
C
200 nm
D
20 nm
E
Fe3O4(311)
d=0.253
(004)
(100)
(311)
(220)
Fe3O4(220)
d=0.297
GR(100)
d=0.216
5 nm
F
C
Fe
Fe
O
Cu
Cu
Fe
Cu
0
5
10
15
20
25
Energy(keV)

Fig. 2

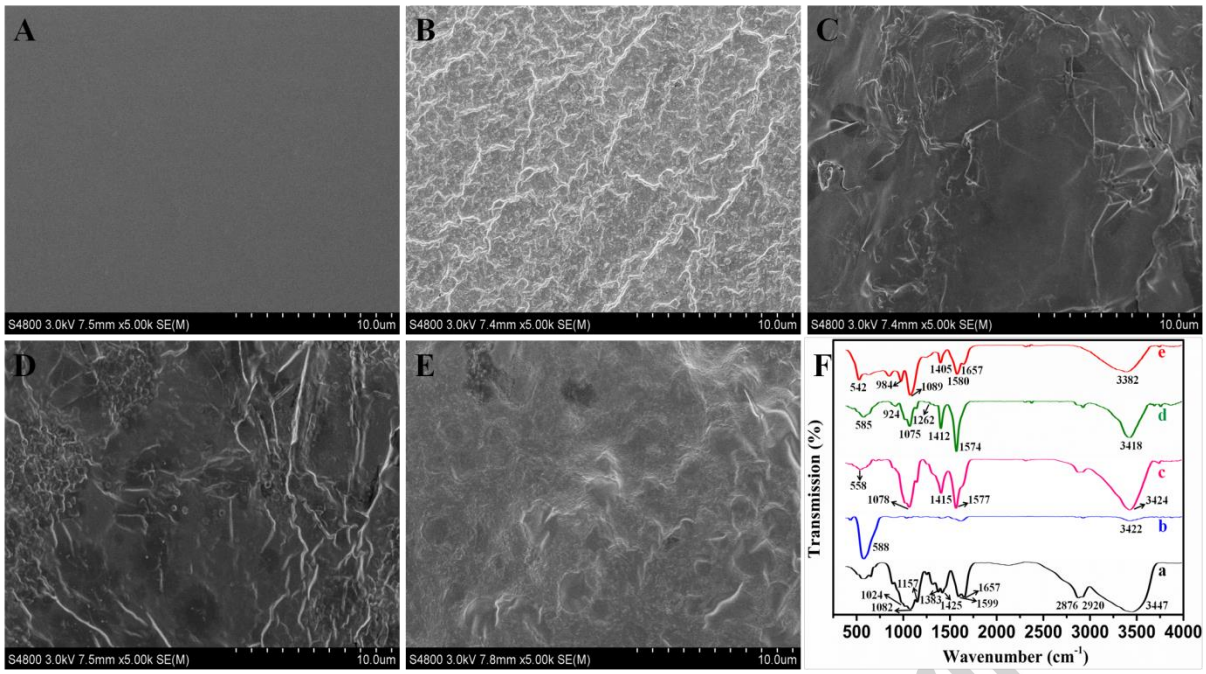

Fig. 3

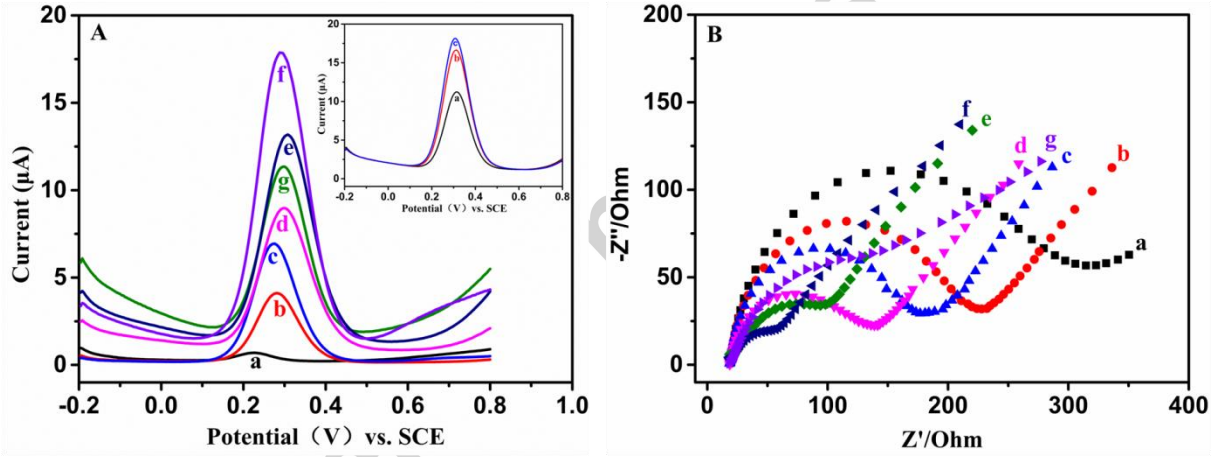

Fig. 4

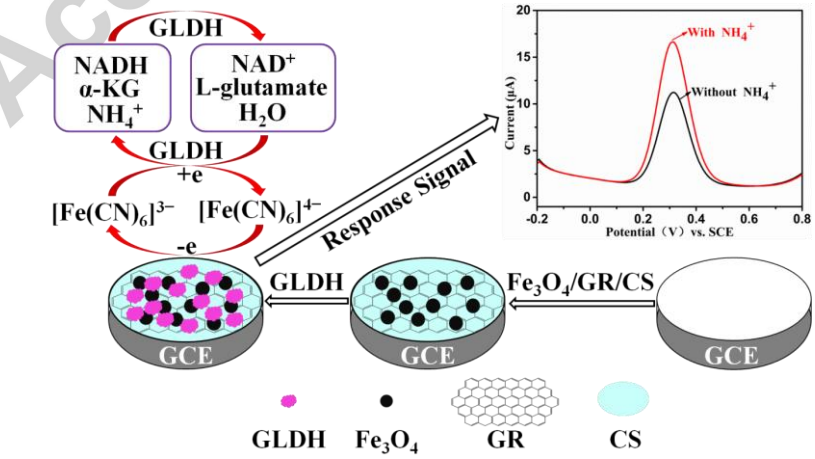

Fig. 5

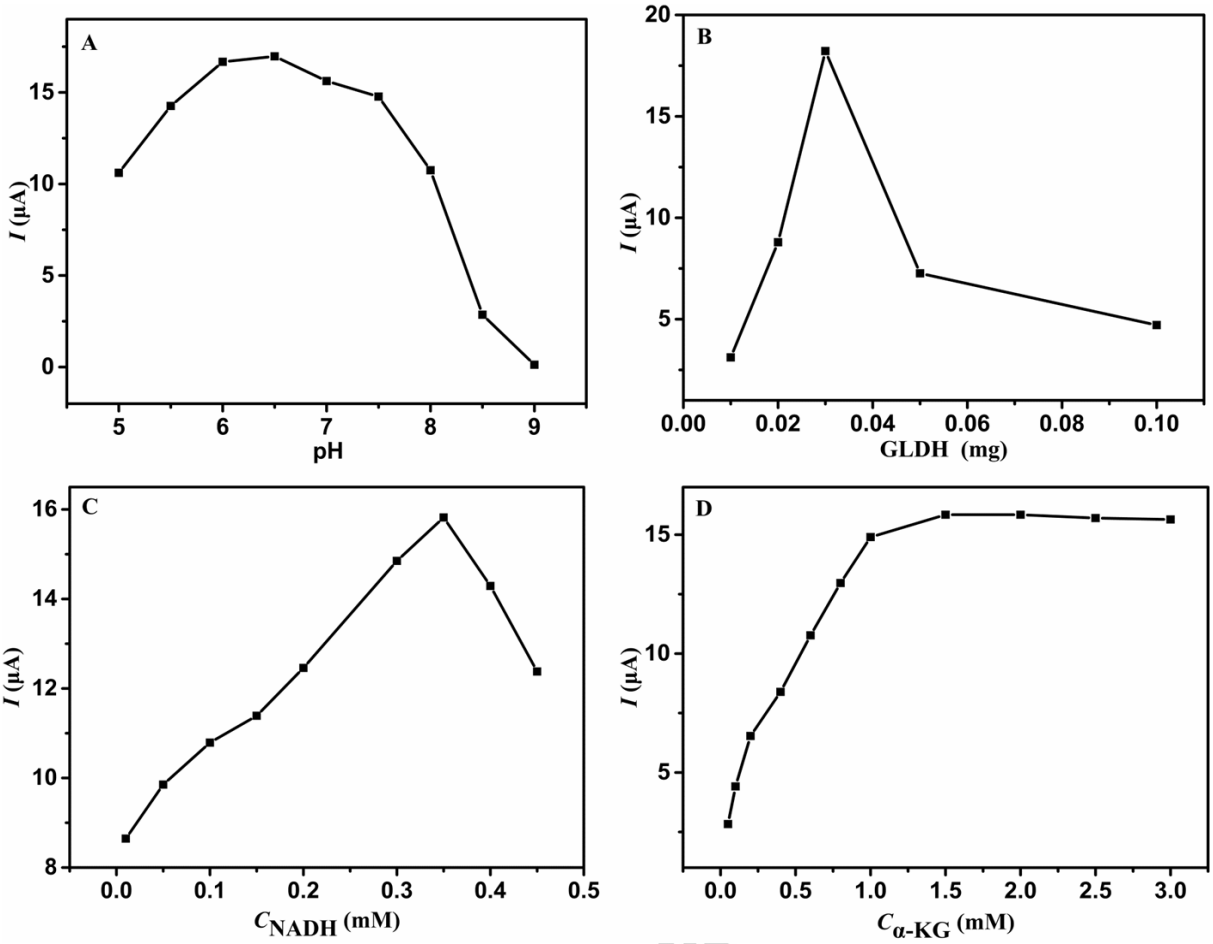
A
I (μA)
pH
B
I (μA)
GLDH (mg)
C
I (μA)
C_{NADH} (mM)
D
I (μA)
$C_{α\text{-}KG}$ (mM)

Fig. 6

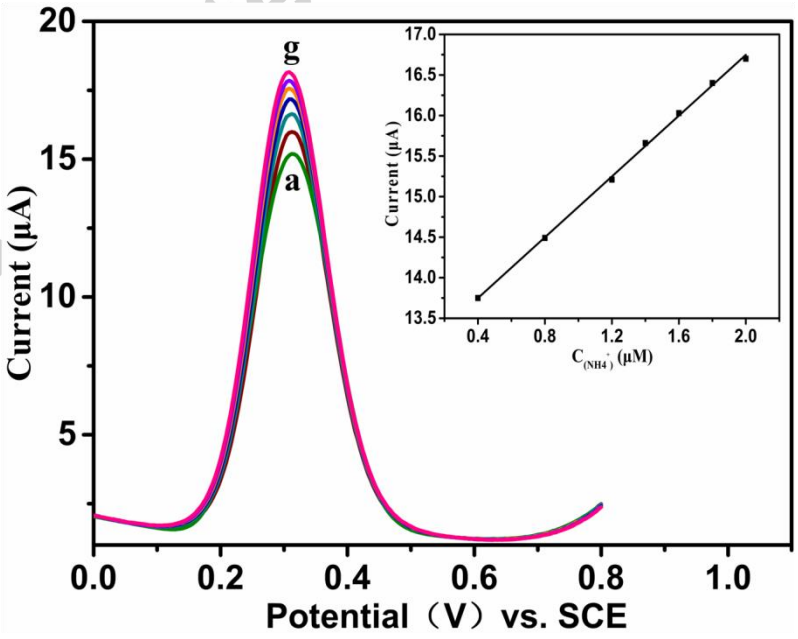
g
a
Current (μA)
Potential（V）vs. SCE
Current (μA)
$C_{(NH4^+)}$ (μM)

Fig. 7

Table 1 Comparison of the proposed biosensor with other GLDH-based NH_4^+ biosensors.

Electrode construction	Linear range (μM)	LOD (μM)	Ref.
GLDH coupled with Pt electrode	10–300	10	[43]
GLDH-CS/diaphorase-CS/SPCE[a]	2.5–500	2.5	[47]
PM[b]/MB[c]/SPCE	1.7–250	1.7	[48]
GXD[d]-GLDH/PCS[e]/Teflon/Clark-type oxygen electrode	10–300	2.06	[49]
GLDH/α-KG/NADH/MB/SPCE	55.56–555.56	55.56	[50]
GLDH/Fe_3O_4/GR/CS/GCE	0.4–2.0	0.08	Present work

[a]SPCE: screen printed carbon electrode; [b]PM: polycarbonate membrane; [c]MB: Meldola's Blue; [d]GXD: glutamate oxidase; [e]PCS: poly(carbamoyl) sulfonate.

Table 2 Determination of NH_4^+ in $PM_{2.5}$ samples (mean ± standard deviation μg/m^3) (n=3).

Sample	EC[a]			IC[b] (μg/m^3)
	Added (μg/m^3)	Found (μg/m^3)	Recovery (%)	
1	0	5.64±0.19	-	5.49±0.06
	2.00	7.67±0.26	101.5	
2	0	4.23±0.14	-	4.11±0.03
	2.00	6.27±0.21	102.0	
3	0	2.11±0.07	-	2.02±0.03
	1.20	3.32±0.08	100.8	

EC[a]: electrochemical method; IC[b]: ion chromatography.

Highlights

- Fe_3O_4/graphene/chitosan nanocomposite was synthesized and characterized.
- The proposed composite provided a good loading platform for glutamate dehydrogenase.
- NH_4^+ in $PM_{2.5}$ was successfully assayed by the developed biosensor.
- This biosensor provided a convenient and low-cost method for NH_4^+ detection in $PM_{2.5}$.